

## Role of Cerium Doping on Epitaxial Yttrium Iron Garnet Thin films

Fida Mohmed<sup>1</sup>, Syed Irfan<sup>1</sup>, Ashiq H Sofi<sup>2</sup>, Farooq A Dar<sup>2</sup>, Majid Hussain<sup>1</sup>, Abid Ahmad<sup>1</sup> and Yuan-Hua Lin<sup>1\*</sup>

<sup>1</sup>State Key Lab of New Ceramics and Fine Processing, School of Materials Science and Engineering, Tsinghua University, Beijing, 100084, PR China

<sup>2</sup>National Institute of Technology, Srinagar, Kashmir, 190006, India

### Abstract

The present work discusses the growth optimization and magnetic properties of the Cerium doped Yttrium Iron Garnet (YIG) thin films grown through Pulsed Laser Deposition technique. The X-ray diffraction (XRD) reveals the highly crystalline, Single Phase, nature of films and the Atomic Force Microscopy (AFM) shows the films are very smooth, with root mean square roughness of less than 1 nm. Thickness of the films as calculated from the X-ray reflectivity (XRR) was found to be around 17, 35, 52, 70 and 122 nm. The Magnetic measurement shows the increase in the Saturation Magnetization, in the cerium doped YIG, but as the growth time increases, we observed a decrease in magnetic Saturation. The decrease in saturation magnetization arises due to the formation of residual Ce<sub>2</sub>O phase in the longer grown films. Longitudinal Spin Seebeck Voltage signal was observed in the films and the Platinum (Pt) deposited over the Cerium doped YIG film showed no sign of Pt magnetization.

**Keywords:** Cerium; Microwave technology; Surface topography; Helmholtz coil

### Introduction

Yttrium Iron Garnet (YIG), has been a highly promising ferromagnetic insulator in the field of microwave sensors, from past many decades because of its large Faraday constant and very low Magnetic damping. Because of these properties YIG is taking its place in the study of Spin waves, Magneto Optic effect and Magnetic Insulator Based Spintronics [1-3]. YIG has a Cubic lattice structure with lattice constant of 12.376 Å, and shows cubic Magneto-crystalline anisotropy with easy axis along (111) direction. The insulating property makes it an ideal candidate for the study of Inverse Spin Hall Effect [4,5], Spin Seebeck Effect [6-9] and pure spin currents [10-12]. In recent years, with the development in microwave technology, Yttrium iron garnet (YIG), cerium-substituted YIG, and bismuth-substituted YIG have engendered substantial interest in spintronics research because of their extraordinary properties like high transparency, large Faraday rotation and excellent magneto-optical characteristics [13,14]. Yttrium iron garnet (YIG) finds numerous applications especially in microwave filters [15,16], microwave sensors [17,18], magneto-optic isolators in telecommunication devices [19,20] etc., due its low magnetic damping, soft magnetization behavior, energy band gap of 2.66 eV, good insulating performance and remarkable combination of low absorption in the optical and near-infrared wavelength region and magneto-optic Faraday effect (FE) [13]. Among the wide variety of applications, several studies revealed that the cerium doped YIG epitaxial films synthesized by liquid phase epitaxy (LPE), traveling solvent floating zone (TSFZ) method, pulsed laser deposition method (PLD), radio frequency (RF) sputtering and the floating zone method using YAG laser heating, enhances the Faraday effect (FE), minimizes optical losses, displaying excellent performance in near-IR wavelength region and maintains its electrical insulating property without much alternation in magnetic moments [21-24]. In the present study, we explore the crystallinity, surface topography and magnetic characteristics of cerium doped YIG thin films (5 mm×5 mm) deposited by pulsed laser deposition method on gadolinium gallium garnet (GGG) substrates in relation to the deposition time and film thickness. A prominent variation in the properties has been observed which have been investigated in detail. The Longitudinal Spin Seebeck voltage signal measurements have also been carried out after depositing the Platinum (Pt) layer over the Cerium doped YIG films.

### Experimental Method

Thin films of YIG and cerium doped YIG (Ce<sub>0.6</sub>Y<sub>2.4</sub>Fe<sub>5</sub>O<sub>12</sub>) have been deposited using pulsed laser deposition technique (PLD) on gadolinium gallium garnet (GGG-111) substrates from mixed powder targets of cerium oxide (Ce<sub>2</sub>O), ytterbium oxide (Y<sub>2</sub>O<sub>3</sub>) and iron oxide (Fe<sub>2</sub>O<sub>3</sub>). All the materials are of high purity (99.99%) and were used as such without any further purification. The powdered mixture of the precursors of stoichiometric weights were grinded to a fine power in ball milling using zirconium oxide (ZrO<sub>2</sub>) balls in a vacuum atmosphere for about 24 hours. The finely grinded powdered mixture was casted into the pellets of 1-inch diameter using cold press followed by sintering at 1400°C for about 12 hours. For the deposition of YIG and CeYIG thin films, the optimum growth conditions were established by maintaining a substrate temperature of 900°C, oxygen pressure of 6.67×10<sup>-3</sup> mbar (5 mtorr) and using a krypton fluoride (KrF, λ=248 nm) laser of pulse energy 120 mJ at a repetition rate of 10 Hz, so that a growth rate of around 3.5 nm/min, could be achieved. Once the deposition process was accomplished the films were allowed to attain the room temperature at a ramp rate of 10 degrees per min until the substrate reaches the room temperature, when the heater was turned off. The substrate to target distance was kept at 7.5 cm for all the films in order to achieve the smooth and uniform film growth. Ex-citu annealing was carried only for pure YIG film using Rapid Thermal Annealing (RTA) in an ambient oxygen flow at 850°C for 300 Sec. A 10 nm Platinum (Pt) film was deposited on the characterized films using magnetron sputtering.

### Results and Discussion

#### Structural properties

For phase, purity and film structure x-ray diffraction (XRD) pattern

**\*Corresponding author:** Lin YH, State Key Lab of New Ceramics and Fine Processing, School of Materials Science and Engineering, Tsinghua University, Beijing, 100084, PR China, Tel: +86 10 6279 3001; E-mail: linyh@mail.tsinghua.edu.cn

Received May 22, 2017; Accepted June 02, 2017; Published June 12, 2017

**Citation:** Mohmed F, Irfan S, Sofi AH, Dar FA, Hussain M, et al. (2017) Role of Cerium Doping on Epitaxial Yttrium Iron Garnet Thin films. J Powder Metall Min 6: 171. doi:10.4172/2168-9806.1000171

**Copyright:** © 2017 Mohmed F, et al. This is an open-access article distributed under the terms of the Creative Commons Attribution License, which permits unrestricted use, distribution, and reproduction in any medium, provided the original author and source are credited.

of the YIG and CeYIG thin films were recorded using Rigaku rotating anode high brilliance (RU-200BH, serial-L17171) diffractometer equipped with Cu K $\alpha$  ( $\lambda=0.15141$  nm) (Mo K $\alpha$  { $\lambda=0.071$  nm}) for XRR) radiation operated at 60 kV and 200 mA. The XRD pattern shown in Figure 1, over  $2\theta$  range of 40-120 degrees, reveals two prominent peaks at 51.11° and 119.09° corresponding to (444) and (666) planes of GGG and CeYIG demonstrating extremely aligned growth of CeYIG on GGG substrates. No other prominent peak corresponding to any impurity could be ascertained revealing the high phase purity of the samples. The film thickness as calculated from the X-Ray reflectivity (XRR) data comes out to be 17.5 nm, 35 nm, 52.5 nm, 70 nm, and 120.5 nm respectively, by using Debye-Scherrer formula  $D = \frac{k\lambda}{\beta \cos\theta}$ , where  $k$  is the shape factor (0.9),  $\lambda$  is the wavelength of the x-ray radiation ( $\lambda=1.5406$  Å),  $\theta$  is scattering angle, and  $\beta$  represents broadening of the diffraction line peak at an angle of  $2\theta$ , at half its maximum intensity (FWHM) in radian [25]. It is obvious that the crystallite size and crystallinity of the films increases as the deposition time increases from 5 to 35 minutes.

### Atomic force microscopy

The surface morphology study was carried out using Asylum 3d-PF Atomic Force Microscope by Oxford Instruments. Figure 2a and 2b displays the AFM images for the Ce doped YIG film we can observe highly smooth, droplet free surface. The root mean square (rms)

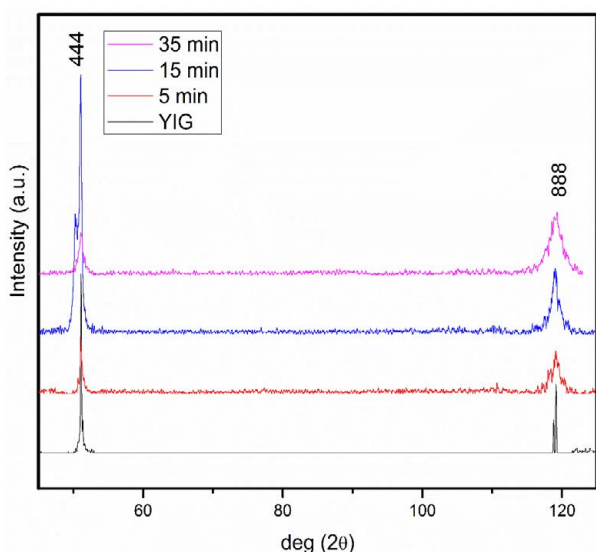


Figure 1: Shows the XRD pattern for the pure and Ce doped YIG films.

roughness of the films as obtained from the AFM is given in the Table 1. The root mean square roughness has increased with film thickness but has remained below 1 nm.

### Magnetic properties

The saturation magnetization calculated from the Super Conducting Quantum Interference Device (SQUID) is presented in Table 1. The Magnetic moment has been calculated after subtracting the background magnetization of the GGG substrate through linear interpolation. The Figure 3a shows the magnetization hysteresis acquired from the SQUID measurement. The magnetic moment of pure YIG film is nearly closer to the addressed value of 145 kA [26-28], but we can observe the increase in saturation magnetization in the cerium doped YIG reaching around 188 kA for 52.5 nm film. The enhanced magnetization in cerium doped YIG was also observed in the Magneto-optic Kerr effect (MOKE) data as shown in the Figure 3b. This increased value of the magnetic moment in the cerium doped YIG as compared to that of pure YIG can be explained by the coupling of the magnetic moments of the Ce<sup>3+</sup> and Fe<sup>3+</sup> ion sublattices. The sublattices “d” site and “a” site of Fe<sup>3+</sup> ions are anti-ferromagnetically coupled. In case of pure YIG Y<sup>3+</sup> does not possess magnetic moment while as “d” site dominates net magnetic moment. The higher magnetic moment of Ce doped YIG is because of Parallel arrangement of Ce<sup>3+</sup> ions to that of “d” sites of Fe<sup>3+</sup> ions [29,30]. Comparing the pure YIG film with the CeYIG films it is clearly indicated in the graph obtained from SQUID Measurements that CeYIG shows larger value of coercive field than that of pure YIG. The coercivity shows increasing trend up to certain deposition time after that it decreases [31]. As the growth time increased beyond 30 minutes, we observe a decrease in both Coercivity and saturation magnetization for the cerium doped YIG. The saturation magnetic moment for 122 nm film was found to be around 168 kA. This decrease in magnetization as the growth time increases is the result of the formation of residual CeO<sub>2</sub> phase within the film which lowers the net magnetic moment.

The Magnetic Anisotropy, which plays an important role in the

Ce:YIG	Film thickness (cm) (error ±3 cm)	Growth time (minutes)	Film roughness (nm)	Saturation Magnetization (kA/m)
Pure YIG	52	20 min	0.32 nm	148.21
Ce:YIG	17.5	5 min	0.21 nm	178.08
Ce:YIG	35	10 min	0.28 nm	184.14
Ce:YIG	52.5	15 min	0.35 nm	188.21
Ce:YIG	70	20 min	0.41 nm	182.12
Ce:YIG	122.5	35 min	0.52 nm	168.38

Table 1: Film thickness, growth time, roughness and saturation magnetization for pure and Ce doped YIG (100) films.

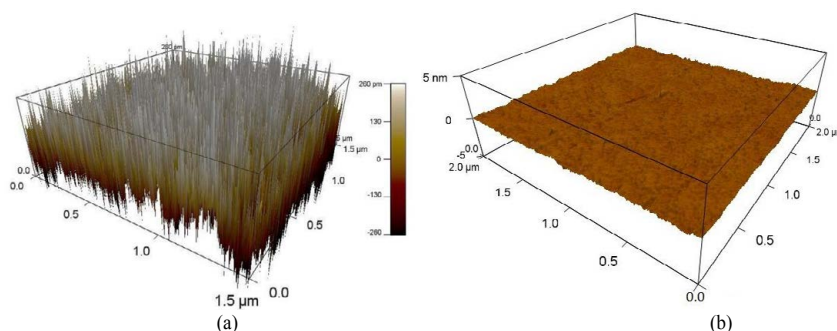


Figure 2: Shows the AFM morphology of the 52.5 nm thick Ce doped YIG films.

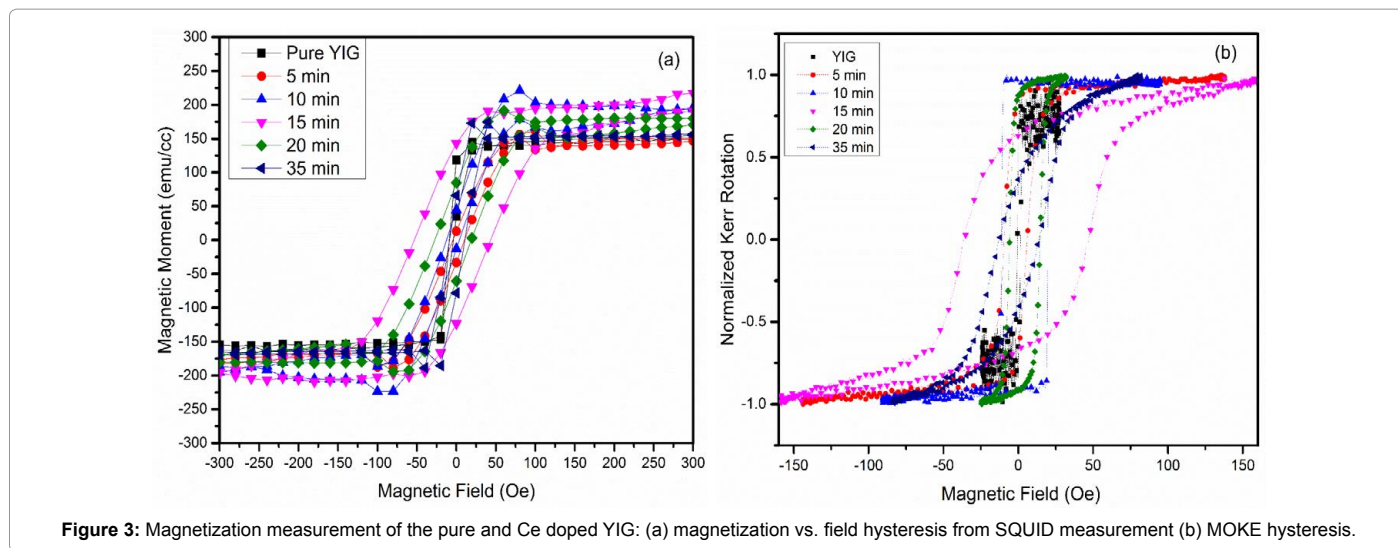


Figure 3: Magnetization measurement of the pure and Ce doped YIG: (a) magnetization vs. field hysteresis from SQUID measurement (b) MOKE hysteresis.

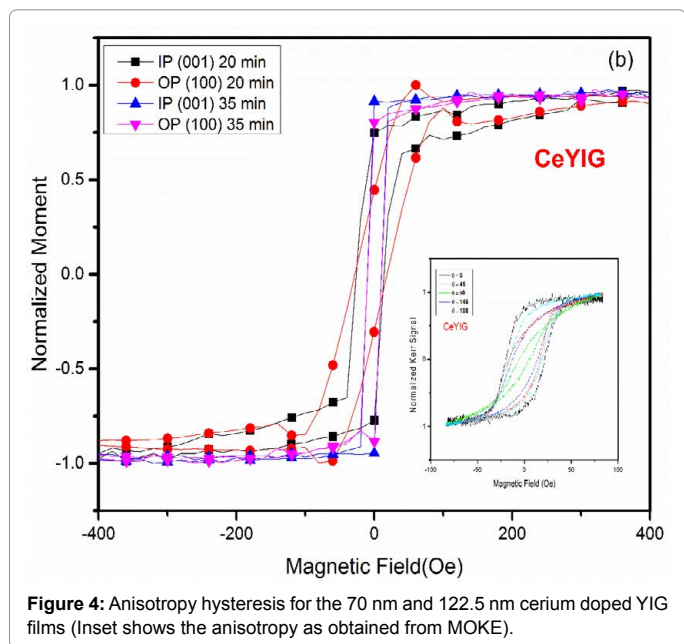


Figure 4: Anisotropy hysteresis for the 70 nm and 122.5 nm cerium doped YIG films (Inset shows the anisotropy as obtained from MOKE).

application of the magnetic materials, has also been observed in our films. The Magnetic anisotropy, compiles from the sum of shape anisotropy, magnetic crystalline anisotropy and uniaxial anisotropy [32]. In case of YIG, it is the weak magnetic crystalline anisotropy which plays the predominant role. Figure 4 shows the hysteresis of magnetic anisotropy for the Ce doped YIG films for 70 nm and 122 nm thin films. The Ce doped YIG shows a stronger magnetic Crystalline anisotropy with easy axis along (111) direction (in-plane) and hard axis along (001) direction (out of plane) magnetization. The anisotropic behavior of the Ce doped YIG was observed in our MOKE results also. The inset of the Figure 4 shows the magnetic anisotropy for the Ce doped YIG film as observed in the MOKE with the angle variation in measurement from 0° to 180°.

### Spin seebeck voltage measurement

In order to observe the Longitudinal Spin Seebeck effect (LSSE) Voltage, a setup needs to be designed wherein we can provide a stable temperature gradient along the longitudinal direction  $\Delta T$ , a varying

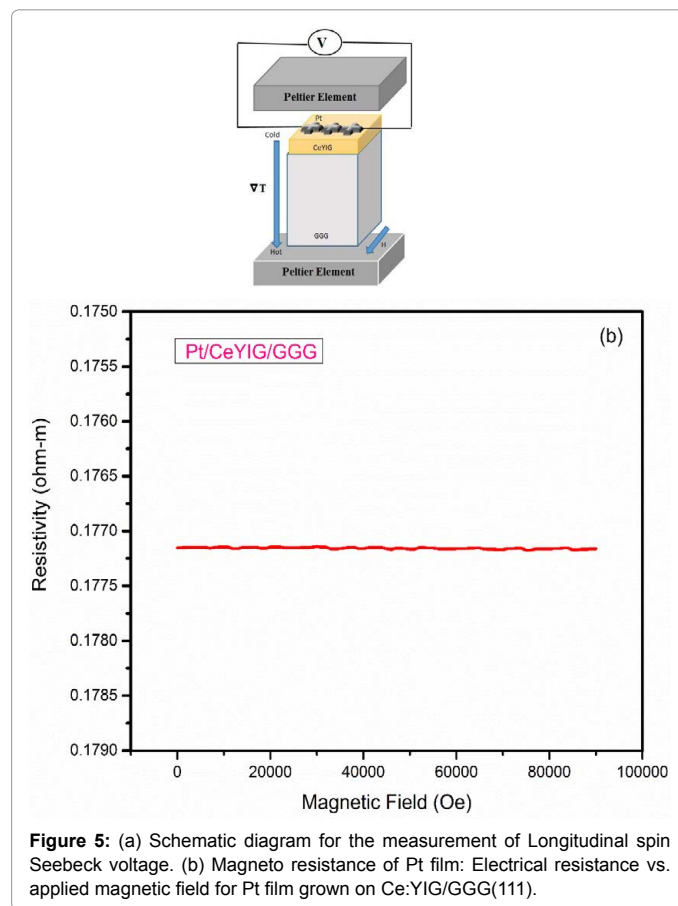


Figure 5: (a) Schematic diagram for the measurement of Longitudinal spin Seebeck voltage. (b) Magneto resistance of Pt film: Electrical resistance vs. applied magnetic field for Pt film grown on Ce:YIG/GGG(111).

magnetic Field  $\vec{H}$  and an instrument to measure the low voltage signal [33]. Figure 5a shows the design of the setup used to measure the LSSE signal in our lab. The stable temperature gradient was provided by two Peltier elements whose temperature was monitored and controlled by using Pt-100 sensors. The Helmholtz coil was used to provide a varying magnetic field. The Spin Seebeck voltage signal generated in the film was measured using a nano Keithley 2182/A nano voltmeter. When a temperature gradient of 10 degrees was maintained between the top Pt layer and the bottom GGG substrate, by sandwiching the

film between two Peltier elements, under the influence of a magnetic field of 100 Oe, a weak Spin Seebeck voltage signal was observed. When the direction of the magnetic field was reversed, the signal direction changed to negative, implying that the generated signal is spin Seebeck voltage. In order to further verify that the signal generated is from the Ce doped YIG and the Pt has not been magnetized, generally known as the magnetic proximity effect [34], the Magnetoresistance (MR) measurement on the Pt film was carried out, using Quantum Design Physical Property Measurement System (PPMS). The Figure 5b shows the room temperature MR vs. H data for the GGG/CeYIG/Pt film. No signs of MR effect was observed in the films, implying that the signal observed is from the spin Seebeck effect in the Ce doped YIG film and the Pt has not been magnetized [35].

## Conclusion

In summary we have obtained a higher magnetic saturation in Ce doped epitaxial pulsed laser deposited YIG films. The films are single phase with very low roughness (with rms <1 nm). The Ce doped YIG films show a saturation magnetization of around 180 emu/cc (5% error), with in-plane easy axis, but as the growth time increased beyond 30 minutes, we observed a dip in saturation magnetization, which occurs due to formation of residual CeO<sub>2</sub>. More over the magnetoresistance measurement of Pt/CeYIG/GGG indicates that the Pt deposited over CeYIG has not been magnetized.

## References

1. Uchida K, Ishida M, Kikkawa T, Kirihara A, Murakami T, et al. (2014) Longitudinal spin Seebeck effect: from fundamentals to application. *J. Phys Condens Matter* 26: 389601.
2. Jaworski CM, Yang J, Mack S, Awschalom DD, Heremans JP, et al. (2010) Observation of spin Seebeck effect in a ferromagnetic semiconductor. *Nature Materials* 9: 898-903.
3. Valenzuela SO, Tinkham M (2006) Direct electronic measurement of the spin Hall Effect. *Nature* 442: 176-179.
4. Uchida K, Takahashi S, Harii K, Ieda J, Koshibae W, et al. (2008) Observation of the spin Seebeck effect. *Nature* 455-459.
5. Uchida K, Xiao J, Adachi H, Ohe J, Takahashi S, et al. (2010) Spin Seebeck Insulator. *Nature Materials* 9: 894-897.
6. Kato YK, Myers RC, Gossard AC, Awschalom DD (2004) Observation of the Spin Hall Effect in Semiconductors. *Science* 306: 1910-1913.
7. Kirihara A, Uchida K, Kajiwara Y, Ishida M, Nakamura Y (2012) Spin Current driven thermoelectric coating. *Nature Materials* 11: 686-689.
8. Adachi H, Uchida K, Saitoh E, Ohe J, Takahashi S, et al. (2010) Gigantic Enhancement of spin Seebeck effect by phonon drag. *Appl Phys Lett* 97: 252506.
9. Uchida K, Adachi H, An T, Ota T, Toda M (2011) Long range spin Seebeck effect and acoustic spin pumping. *Nature Materials* 10: 737-741.
10. Li P, Ellsworth D, Chang H, Janantha P, Richardson D, et al. (2014) Generation of pure spin currents via spin Seebeck effect in self-biased hexagonal ferrite thin films. *Appl Phys Lett* 105: 242412.
11. Jia X, Liu K, Xia K, Bauer GEW (2011) Spin transfer torque on magnetic insulators. *Europhys Lett* 96: 17005.
12. Xiao J, Bauer GEW, Uchida K, Saitoh E, Maekawa S (2010) Theory of magnon-driven spin Seebeck effect. *Phys Rev B* 81: 214418.
13. Kehlberger A, Richter K, Onbasli MC, Jakob G, Kim DH, et al. (2015) Enhanced Magneto-optic Kerr Effect and Magnetic Properties of CeY<sub>2</sub>Fe<sub>5</sub>O<sub>12</sub> Epitaxial Thin Films. *Physical Review Applied* 4: 014008.
14. Goto T, Onbasli MC, Ross CA (2012) Magneto-optical properties of cerium substituted yttrium iron garnet films with reduced thermal budget for monolithic photonic integrated circuits. *Optics Express* 20: 28507-28517.
15. Röschmann P (1973) Compact YIG bandpass filter with finite-pole frequencies for applications in microwave integrated circuits. *IEEE Trans. Microwave Theory Tech* 21: 52 - 57.
16. Deeter MN, Rose AH, Day GW (1990) Fast sensitive magnetic-field sensors based on the Faraday effect in YIG. *J Lightwave Technol* 8: 1838-1842.
17. Murakami Y, Ohgihara T, Okamoto T (1987) A 0.5-4.0 GHz tunable bandpass filter using YIG film grown by LPE. *IEEE Trans Microwave Theory Tech* 35: 1192.
18. Higuchi S, Ueda K, Yahiro F, Nakata Y, Uetsuhara H, et al. (2001) Fabrications of cerium-substituted YIG thin films for magnetic field sensor by pulsed-laser deposition. *IEEE Trans Magn* 37: 2451-2453.
19. Stadler BJH, Mizumoto T (2014) Integrated magneto-optical materials and isolators: A review. *IEEE Photonics J* 6.
20. Shoji Y, Mizumoto T, Yokoi H, Hsieh IW, Osgood RM (2008) Magneto-optical isolator with silicon waveguides fabricated by direct bonding. *Appl Phys Lett* 92: 071117.
21. Shintaku T, Tate A, Mino S (1997) Ce-substituted yttrium iron garnet films prepared on GdScGaO garnet substrate by sputter epitaxy. *Appl Phys Lett* 71: 12-1640.
22. Tamanoi K, Ariizumi M, Shinagawa K, Saito T, Tsushima T (1989) Faraday effects of cerium-substituted YIG LPE films. *J Magn Soc Jpn* 13: 44-45.
23. Sekijima T, Funakoshi T, Katabe K, Tahara K, Fujii T, et al. (1998) Growth and optical properties of Ce-substituted fibrous YIG single crystals. *Jpn J Appl Phys* 37: 4854.
24. Higuchi S, Furukawa Y, Takekawa S, Kamada O, Kitamura K (1999) Magneto-optical properties of cerium-substituted yttrium iron garnet crystals grown by traveling solvent floating zone method. *Jpn J Appl Phys* 37: 4854.
25. Gagaoudakis E, Bender M, Douloufakis E, Katsarakis N, Natasakou E (2001) *Sensors and Actuators B* 80: 105.
26. Siegel G, Prestgard MC, Teng S, Tiwari A (2014) Robust longitudinal spin-Seebeck effect in Bi-YIG thin films. *Scientific reports* 4: 4429.
27. NIST X-ray photoelectron spectroscopy database. Measurement Services Division of the National Institute of Standards and Technology (NIST) Technology Services, 2008.
28. Onbasli MC, Kehlberger A, Kim DH, Jakob G, Kläui M, et al. (2014) Pulsed Laser deposition of epitaxial yttrium iron garnet films with low Gilbert damping and bulk like magnetization. *APL Materials* 2: 106102.
29. Xu H, Yang H (2008) Magnetic properties of YIG doped with cerium and gadolinium ions. *J Mater Sci* 19: 589.
30. Sekijima T, Kishimoto H, Fujii T, Wakino K, Okada M (1999) Magnetic, optical and microwave properties of rare-earth-substituted fibrous yttrium iron garnet single crystals grown by floating zone method. *Jpn J Appl Phys* 38: 5874.
31. Mao TC, Chen JC (2006) Influence of the addition of CeO<sub>2</sub> on the microstructure and the magnetic properties of yttrium iron garnet ceramic. *J Magn Mater* 302: 74-81.
32. Chern MY, Liaw JS (1997) Study of Bi<sub>x</sub>Y<sub>3-x</sub>Fe<sub>5</sub>O<sub>12</sub> Thin Films Grown by Pulsed Laser Deposition. *Jpn J Appl Phys* 36.
33. Schmid M (2015) Magneto-thermoelectric effects in NiFe thin films, thesis Universitätsverla Regensburg.
34. Lu YM, Choi Y, Ortega CM, Chien CL, Cai JW, et al. (2013) Pt Magnetic Polarization on Y<sub>3</sub>Fe<sub>5</sub>O<sub>12</sub> and Magneto transport Characteristics. *Physical Review Letters* 110: 147207.
35. Miao BF, Huang SY, Qu D, Chien CL (2014) Physical Origins of the new Magnetoresistance in Pt/YIG. *Phys Rev Lett* 112: 236601.

Citation: Mohmed F, Irfan S, Sofi AH, Dar FA, Hussain M, et al. (2017) Role of Cerium Doping on Epitaxial Yttrium Iron Garnet Thin films. J Powder Metall Min 6: 171. doi:10.4172/2168-9806.1000171